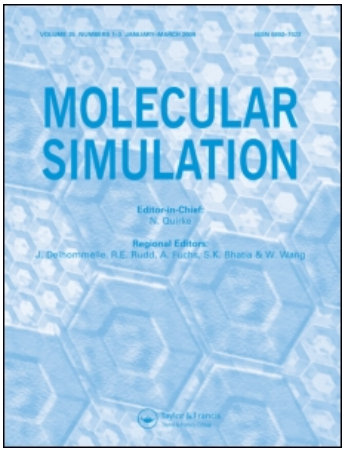

Molecular Simulation
Publication details, including instructions for authors and subscription information:
http://www.informaworld.com/smpp/title~content=t713644482

Kinetic Monte Carlo study on transient enhanced diffusion: *posterior to* amorphisation process

Soon-Yeol Park[a]; Young-Kyu Kim[a]; Taeyoung Won[a]
[a] Department of Electrical Engineering, School of Information Technology Engineering, Inha University, Incheon, Republic of Korea

To cite this Article Park, Soon-Yeol , Kim, Young-Kyu and Won, Taeyoung(2009) 'Kinetic Monte Carlo study on transient enhanced diffusion: *posterior to* amorphisation process', Molecular Simulation, 35: 6, 525 — 529
To link to this Article: DOI: 10.1080/08927020902874008
URL: http://dx.doi.org/10.1080/08927020902874008

Molecular Simulation
Vol. 35, No. 6, May 2009, 525–529

Taylor & Francis
Taylor & Francis Group

Kinetic Monte Carlo study on transient enhanced diffusion: *posterior to* amorphisation process

Soon-Yeol Park*, Young-Kyu Kim and Taeyoung Won[1]

Department of Electrical Engineering, School of Information Technology Engineering, Inha University, Incheon 402-751, Republic of Korea

(*Received 31 October 2008; final version received 4 March 2009*)

We report our theoretical investigations on the suppression of boron diffusion in the silicon substrate *posterior to* pre-amorphisation implant (PAI). We numerically investigated the defect-generating behaviour of silicon atoms and their subsequent effect on the transient enhanced diffusion (TED) of boron as a new species for PAI. Our kinetic Monte Carlo simulation revealed that Si–PAI produces more interstitials than the case of Ge–PAI, while Ge–PAI makes interstitial moves further up to the surface than the Si–PAI case during the annealing process, which results in the suppression of the boron TED.

Keywords: transient enhanced diffusion; kinetic Monte Carlo; pre-amorphisation implant

1. Introduction

As devices scale down to the deca-nanometre region, the scaling scenario more stringently requires a shallow source/drain junction profile. Junction depth control is one of the key factors that can alleviate the short channel effect for deca-nanometre-node technologies, especially for high-performance devices. Traditionally, boron has been an important dopant to make p-channel transistors, but boron has a channelling effect during an implant process in the crystalline silicon lattice. Also, impure atoms experience various kinds of scattering events and finally stop their penetration when they lose their energy during the scattering process. Dopant diffusion during the subsequent annealing process, which is called transient enhanced diffusion (TED), is well known to deepen the junction depth [1–3]. To prevent channelling and the TED phenomena, pre-amorphisation implant (PAI) is considered to be an efficient method. The germanium atom has been favourably employed for the PAI process because it reduces the channelling and TED diffusion of B atoms for the formation of a shallow junction. However, since the size of the germanium atom is larger than that of silicon atom, the lattice structure of the silicon substrate is considered to experience the deformation in a more severe and irregular manner. Furthermore, it has been well-known that the boron atoms experience some kind of impurity scattering. In this work, we theoretically investigated the pros and cons for the silicon PAI as an alternative to the traditional Ge–PAI process because silicon atoms are the same species with the silicon substrate and the size of the silicon atoms is smaller than that of the germanium, which might be expected to cause less lattice deformation.

2. Computational details

2.1 Ion implantation

In order to investigate the diffusion phenomena of boron after pre-amorphisation process, we need an as-implant B profile for Si–PAI as well as Ge–PAI. In this work, we employed the BCA code for the initial as-implant dopant profile, which is based upon the Kinchin–Pease model. Kinchin–Pease model is a computationally efficient damage model based on the modified Kinchin–Pease formula proposed by Norgett et al. [4]. In a simplified manner, this model accounts for damage generation, damage accumulation, defect encounters and amorphisation. The basic assumption of the Kinchin–Pease models is the nuclear energy loss which turned into point defects and the number of Frenkel pairs which is created proportionally to the nuclear energy loss. The nuclear energy loss is deposited locally and induces local defects.

2.2 Thermal annealing simulation

After the implant process, we implement the annealing process by using our kinetic Monte Carlo (kMC) code [5,6]. In the kMC method, a physical system which consists of many possible events evolves as a series of independent event occurrences. Each event has its own event rate. Event rate is calculated from the Equation (1). Here, E_b presents the migration energy for the barrier against the jump event of the mobile species or a binding energy for clusters. In addition, v_0 is the attempt frequency which is simply the vibration frequency of the atoms. Typically, the attempt frequency is the order of 1/100 fs.

*Corresponding author. Email: psy@hsel.inha.ac.kr

ISSN 0892-7022 print/ISSN 1029-0435 online

DOI: 10.1080/08927020902874008
http://www.informaworld.com

These parameters can be obtained from the *ab initio* calculation or experimental data.

$$v = v_0 \exp\left(\frac{-E_b}{K_B T}\right). \quad (1)$$

Our problem is the consideration about the thermally activated events in a thermal annealing simulation after ion implantation. If the probability for the next event to occur is independent of the previous history, and the same at all times, the transition probability will be a constant which is called Poisson process. To derive the time dependence, we can consider a single event with a uniform transition probability r. Let f be the transition probability density which gives the probability rate at which the transition occurs at time t. The change of $f(t)$ over a short time interval dt is proportional to r, dt and f because f gives the probability density that the physical system still remains, at time t:

$$df(t) = -rf(t)\,dt. \quad (2)$$

The solution of Equation (2) can be easily obtained as the following wherein r becomes the initial value of $f(t)$:

$$f(t) = re^{-rt}, \quad f(0) = r. \quad (3)$$

Therefore, the simulation time is updated for $(t = t + \Delta t)$ according to event rates as follows, because an ensemble of independent Poisson processes will behave as one large Poisson process:

$$\Delta t = -\frac{\ln u}{R}, \quad R = \sum_{i=1}^{N} R_i. \quad (4)$$

Here, u is a random number and R is the total sum of all possible event rates (R_i). We select an event according to the event rates.

3. Results and discussion

Figure 1 is a schematic which illustrates the simulated B as-implant profile wherein the dotted line represents the as-implant profile without PAI; the scattered squares designate the as-implant profile with Ge–PAI, and the scattered circles represent the as-implant profile with Si–PAI. It should be further noted that the filled circles and squares represent the cases for PAI with implant energy of 20 keV while the empty circles and squares represent the cases for PAI with implant energy of 40 keV. Referring to the as-implant PAI-free B profile (dotted line) and other scattered curves (circulars and squares), we can see that the pre-amorphisation process either with Ge or with Si helps to realise the shallow junction. If we look into the as-implant profiles for each type of PAI species with different implantation energies, we can see that the PAI process with 40 keV is more favourable than the case

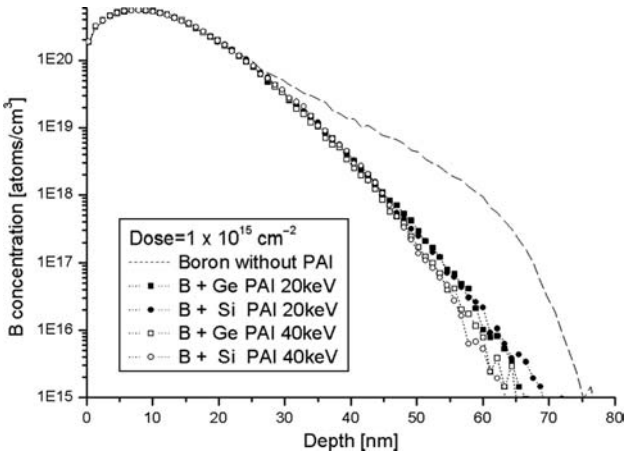

Figure 1. Boron as-implant profiles. Boron is implanted with an energy of 2 keV, a dose of $1 \times 10^{15}/cm^2$ after Si/Ge–PAI is implemented with energies of 20 and 40 keV and a dose of $1 \times 10^{15}/cm^2$. All implantations were performed with 7 tilt angle. The dotted line represents the as-implant profile without PAI, the scattered squares designate the as-implant profile with Ge–PAI and the scattered circles represent the as-implant profile with Si–PAI. It should be further noted that the filled circles and squares represent the cases for PAI with an energy of 20 keV while the empty circles and squares represent the cases for PAI with an energy of 40 keV.

with 20 keV in terms of the depth of the as-implanted B profile. In other words, higher energy PAI seems to retard the boron channelling more effectively regardless of the species of PAI atoms. If we make comments on the species of PAI implant, the as-implant profile with Si–PAI is shallower than that with Ge–PAI.

Figures 2 and 3 are schematics which illustrate the simulated B profile for different annealing conditions wherein Figure 2 corresponds to the thermal annealing for 60 s at 850°C, while Figure 3 corresponds to the RTA for 1 s at 600°C, respectively, for Si–PAI as well as Ge–PAI. PAI implantation was performed with a dose of $1 \times 10^{15}/cm^2$ and with energies of 20 and 40 keV, respectively. Boron implantation is performed with a dose of $1 \times 10^{15}/cm^2$ and with an energy of 2 keV. The solid line represents the B diffusion profile without PAI while the line with squares correspond to the cases with Ge–PAI and the lines with circles represent the cases with Si–PAI.

Referring to Figure 2, we can recognise that there seems to be no significant difference in the diffusion profiles after annealing for 60 s. The reasons seem to be due to the fact that the boron implantation energy is relatively low when compared to the annealing time and temperature. This seems partly due to the fact that a low-energy implantation induces the statistical inaccuracy and further that a long duration annealing at high temperature supplies enough energy for boron diffusion. In order to confirm our reasoning, we performed kMC simulation under the different annealing condition, i.e. under the RTA condition.

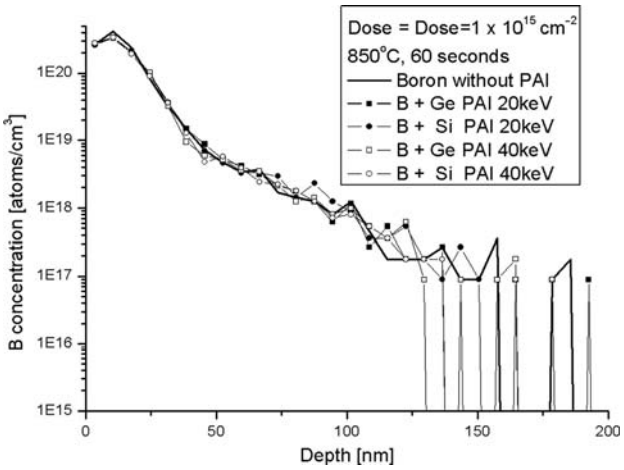

Figure 2. Boron profile after annealing at 850°C for 60 s. The solid line represents the B diffusion profile without PAI while the line with squares corresponds to the cases with Ge–PAI and the lines with circles represent the cases with Si–PAI.

Figure 3 is a schematic illustrating the diffusion profiles after annealing at 600°C for 1 s wherein the notations are the same as the ones used in Figure 2. Referring to Figure 4, we can see that PAI significantly reduces the TED and PAI effect is more pronounced than the case of long time annealing. Moreover, we can see that Si–PAI with energy of 20 keV is better than the other PAI cases with respect to the suppression of diffusion profiles.

In order to understand the physics behind the suppression of diffusion profiles, we investigated the defect (interstitial and vacancy) distribution with our kMC tool, which is depicted in Figures 4 and 5. Figure 4 is a schematic which illustrates the simulated interstitial (I) distribution for Ge–PAI and Si–PAI cases under our

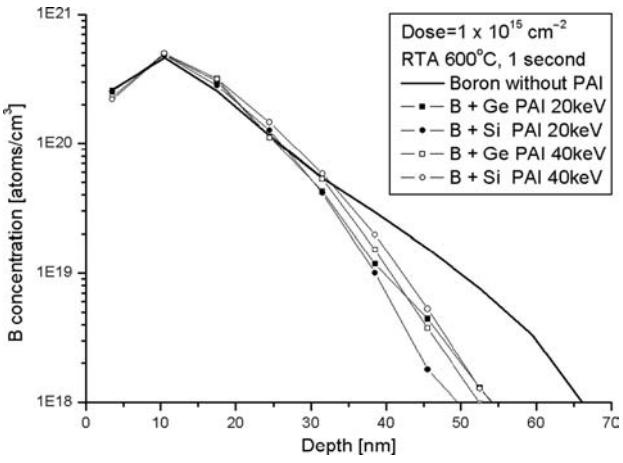

Figure 3. Boron profile after annealing at 600°C for 1 s. The solid line represents the B diffusion profile without PAI while the line with squares corresponds to the cases with Ge–PAI and the lines with circles represent the cases with Si–PAI.

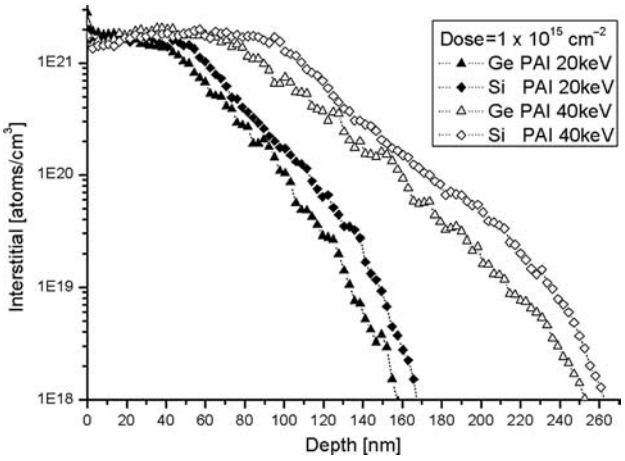

Figure 4. A plot illustrating the simulated interstitial distributions. The triangles represent the case with Ge–PAI wherein the filled triangle represents the case with 20 keV while the empty triangle represents the case with 40 keV. The diamonds represent the case with Si–PAI wherein the filled diamond represents the case with 20 keV while the empty diamond represents the case with 40 keV.

kMC simulation. Here, the triangles represent the case with Ge–PAI wherein the filled triangle represents the case with 20 keV while the empty triangle represents the case with 40 keV. Furthermore, the diamonds represent the case with Si–PAI wherein the filled diamond represents the case with 20 keV while the empty diamond represents the case with 40 keV. Referring to Figure 4, we can recognise that the interstitial distribution for the Si–PAI produces more amounts of interstitial than the

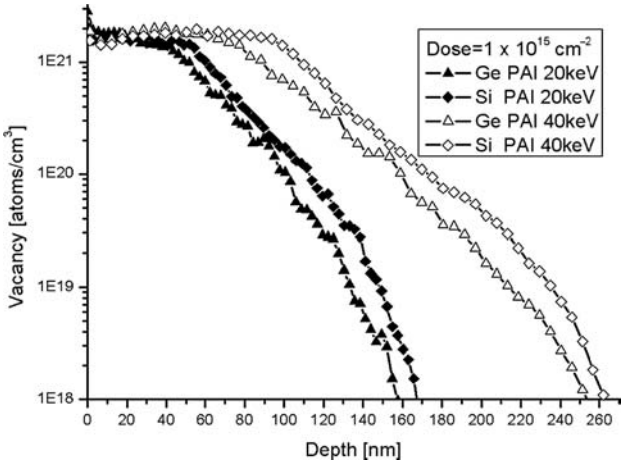

Figure 5. A plot illustrating the simulated Vacancy distributions. The triangles represent the case with Ge–PAI wherein the filled triangle represents the case with 20 keV while the empty triangle represents the case with 40 keV. The diamonds represent the case with Si–PAI wherein the filled diamond represents the case with 20 keV while the empty diamond represents the case with 40 keV.

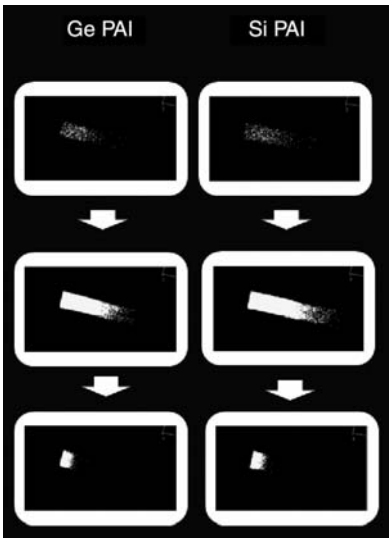

Figure 6. Interstitial distribution changes in terms of annealing time. Finally, interstitials move towards and nearer to the surface in both the PAI and both implantation energies.

Ge–PAI case near the surface, which seems to suppress the boron diffusion more effectively than Ge–PAI [7].

Figure 5 is a diagram which illustrates the simulated vacancy distribution for Ge–PAI and Si–PAI cases according to our kMC simulation. Referring to Figure 5, we can see that the vacancy profile is very similar to the interstitial profile. In this paper, we define the amorphous-crystalline interface by estimating the interstitial distribution. We consider the region to be amorphous if the region's interstitial amounts exceed 1×10^{23}.

Further, we simulated the change in the interstitial distribution using Si atoms as well as Ge atoms as PAI source with a dose of $1 \times 10^{15}/\text{cm}^2$, and with an energy of 40 keV, while the boron implantation energy was 2 keV with a dose of $1 \times 10^{15}/\text{cm}^2$ during the annealing process as shown in Figure 6.

Figure 6 is a schematic which illustrates the three dimensional interstitial distribution. In this figure, we can see that the interstitials produced by Si–PAI are formed more deeply than those of Ge–PAI at the initial stage of the entire procedure while the interstitials move towards the inner depth. Finally, the interstitials are positioned near the surface for both the samples. The kMC simulation in Figure 6 reveals that interstitials induced by Ge–PAI are located more nearer to the surface than the cases of Si–PAI. From this difference in the distribution, we can see that both the PAI processes reduce the boron diffusion as the interstitials move up near to the surface.

In order to verify our kMC simulation, we compared our diffusion profiles with experimental data, which is taken from the previously published literature [8]. Referring to Figure 7, we can see quite a good agreement

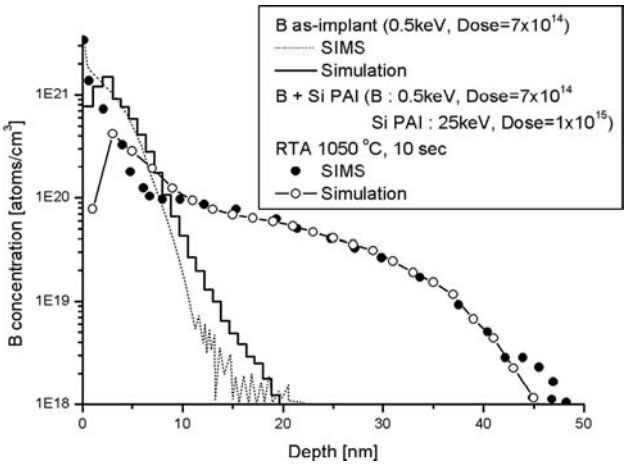

Figure 7. kMC profile with SIMS data for an as-implant B as well as the boron with Si–PAI.

between the simulated boron profile after PAI as well as the as-implant profile and the secondary ion mass spectroscopy (SIMS) data. The numerical verification for Ge–PAI has already been conducted and reported in our previous publication [6].

4. Conclusion

In this paper, we investigated silicon atoms as a new PAI sources in addition to Ge atoms. Our kMC simulation revealed that the Si–PAI process produces more amount of interstitial and vacancy, which reduces the boron TED. We compared the effects of Si–PAI with those of Ge–PAI under the same annealing condition. From the kMC investigation of the interstitial distribution, we found that Si–PAI produces more interstitials than the case of Ge–PAI while Ge–PAI makes interstitials move further to the surface than the Si–PAI case during the annealing process.

Acknowledgements

This research was supported by the Ministry of Knowledge and Economy, Korea, under the Information Technology Research Center (ITRC) support program supervised by the Institute of Information Technology Advancement (IITA) (IITA-2008-C109008010030). This work was supported by an Inha University research grant.

Note

1. Email: twon@hsel.inha.ac.kr

References

[1] P.M. Fahey, P.B. Griffin, and J.D. Plummer, *Point defects and dopant diffusion in silicon*, Rev. Mod. Phys. 61 (1989), pp. 289–384.
[2] P.A. Stolk, H. Gossmann, D.J. Eanglesham, D.C. Jacobson, C.S. Rafferty, G.H. Gilmer, M. Jaraiz, J.M. Poate, H.S. Luftman, and T.E. Haynes, *Physical mechanisms of transient enhanced dopant*

diffusion in ion-implanted silicon, J. Appl. Phys. 81 (1977), pp. 6031–6050.

[3] A. Agarwal, H. Gossmann, D.J. Eaglesham, S.B. Herner, A.T. Fiory, and T.E. Haynes, *Boron-enhanced diffusion of boron from ultralow-energy ion implementation*, Appl. Phys. Lett. 74 (1999), pp. 2435–2437.

[4] M.J. Norgett, M.T. Robinson, and I.M. Torrens, *A proposed method of calculating displacement dose rates*, Nucl. Eng. Des. 33 (1975), pp. 50–54.

[5] J. Yoo, K. Yoon, J. Kim, and T. Won, *Atomistic simulation for a Nano-CMOS process: from ion implementation to diffusion*, J. Korean Phys. Soc. 49(3) (2006), pp. 1260–1265.

[6] J. Kim and T. Won, *Atomistic modelling for boron diffusion profile in silicon posterior to germanium pre-amorphization*, Microelectron. Eng. 84 (2007), pp. 1556–1561.

[7] A. Ural, P.B. Griffin, and J.D. Plummer, *Fractional contributions of microscopic diffusion mechanism, for common dopants and self-diffusion in silicon*, J. Appl. Phys. 85 (1999), pp. 6440–6446.

[8] B.J. Pawlak, T. Janssens, B. Brijs, W. Vandervorst, E.J.H. Collart, S.B. Felch, and N.E.B. Cowern, *Effect of amorphization and carbon co-doping on activation and diffusion of boron in silicon*, Appl. Phys. Lett. 89 (2006), 062110.